# The interaction of CO with Ni(111): Rainbows and rotational trapping

Melissa A. Hines[a] and Richard N. Zare
*Department of Chemistry, Stanford University, Stanford, California 94305*

(Received 21 January 1993; accepted 22 February 1993)

Angularly resolved rotational state distributions of CO scattered and desorbed from a clean, single-crystal Ni(111) surface were measured using (2+1) resonance-enhanced multiphoton ionization. Molecules scattered from the surface displayed highly non-Boltzmann rotational distributions that varied with incident translational energy and detection angle, but not with surface temperature. A rotational rainbow was seen in the scattering distribution and interpreted as arising from the interaction of the weakly attractive O end of the CO molecule with the Ni(111) surface. Up to total rotational-to-translational energy conversion was seen at incident translational energies of 0.26–0.45 eV. This energetic cutoff was the result of rotational trapping and was caused by the strongly attractive interaction of the C end of the molecule with the surface. The rotational state distributions of molecules desorbed from the Ni(111) surface were well fit by Boltzmann distributions each with a temperature which is $0.82 \pm 0.08$ of the surface temperature.

## I. INTRODUCTION

Gas–surface scattering provides unique insight into the dynamics of molecular adsorption. Surface spectroscopies such as photoemission, He scattering, and electron-energy-loss spectroscopy (EELS) are very sensitive probes of the nature of adsorbed species; however, they provide little insight into the actual path a molecule takes from the gas phase to the chemisorbed phase. Direct information about the absorption process has proven to be quite elusive. Consequently, we have taken an indirect approach—instead of studying molecules that adsorb, we studied molecules that do not adsorb, i.e., those that scatter. In a system in which both scattering and adsorption are important channels, the dynamics of the scattering process are complementary to the dynamics of the sticking process. Simply put, if we can first understand how and why certain molecules scatter from a surface, we can then infer why others do not scatter—why they stick. In this way, gas–surface scattering is sensitive to the *early-time dynamics* of the adsorption process.

A variety of techniques have been used to study gas–surface scattering dynamics.[1] In this study, we concentrate on the internal state distribution (almost exclusively the rotational excitation) of molecules scattered from a surface. If the rotational excitation of the incident molecule is negligible, the final rotational state will be determined by the various torques acting on the molecule during scattering. Previous studies of rotationally inelastic scattering in weakly interacting gas/surface systems have proved informative.[2]

We chose to study a seemingly simple system—the adsorption of carbon monoxide (CO) on the flat, close-packed surface of nickel [the Ni(111) surface]. In this system, adsorption is both nondissociative and unactivated.[3,4] This system is not a weakly interacting one, however; the activation energy for desorption ($E_d$) has been measured to be 1.3 eV.[5] Studies by Tang *et al.*[3] showed that for a wide range of incident translational energies $0.3 \leqslant E_{\text{inc}} \leqslant 1.3$ eV, approximately 50% of an incident beam of CO will stick to a Ni(111) surface. Our measurements concentrate almost exclusively on this translational energy regime where scattering and chemisorption are competitive processes.

The chemisorption of CO on metal surfaces is the subject of much research, both theoretical and experimental, and the CO/metal bond is understood comparatively well. Sung and Hoffmann[6] have presented an excellent introduction to this tropic. In brief, CO bonds to a Ni(111) surface in a C-end-down configuration with the C–O bond normal to the surface. The bonding in this system can be understood in terms of the strong interaction of the CO $5\sigma$ and $2\pi$ orbitals with the metal $d$ orbitals. The fact that CO preferentially bonds C end down is a consequence of the electronic structure of the CO molecule—the $5\sigma$ molecular orbital is essentially a carbon lone pair and the $2\pi$ orbital is polarized toward the C end of the molecule.

Because of this strong chemical interaction between the C end of CO and the nickel surface, the CO/Ni(111) potential is highly anisotropic. The binding energy of the O-end-down configuration can be estimated from the interaction of $N_2$ with a nickel surface. On the basis of their steady-state Fourier transform infrared (FTIR) studies, Yoshinobu *et al.*[7] estimated the enthalpy of adsorption of $N_2$ on Ni(111) to be 0.35 eV. This is approximately 1 eV weaker than the Ni–CO bond and implies that the O-end-down configuration of CO on Ni(111) is bound by only $\approx$0.35 eV.

Because of this strongly anisotropic interaction, only the region of the potential near the C-end-down configuration is important in determining equilibrium properties. In contrast, we shall show that scattering is sensitive to the entire potential. The reason is clear—molecules incident on the surface from the gas phase are randomly oriented and, though there is a strong attractive interaction between CO

[a]Present Address: AT&T Bell Laboratories, 600 Mountain Ave., Murray Hill, NJ 07974.

 0021-9606/93/119134-14$06.00 

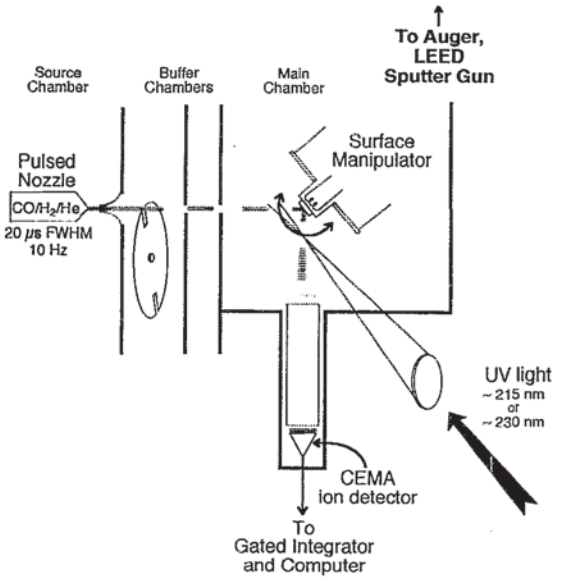


FIG. 1. A schematic diagram of the experimental apparatus.

and the Ni(111) surface, there is insufficient time for the CO molecule to significantly reorient prior to collision with the surface. In this study, we will show that molecules that hit the surface O end down have quite different dynamics than those that hit C end down. O end collisions preferentially lead to scattering, while C-end collisions preferentially lead to chemisorption. These results show clearly that a simple one-dimensional representation of the interaction of CO with Ni(111) is a vast oversimplification that represents, at most, an average interaction potential.

## II. EXPERIMENT

These experiments were performed in an ultrahigh vacuum (UHV) chamber described previously.[8–10] The apparatus is shown schematically in Fig. 1. Briefly, a pulsed, chopped supersonic molecular beam of carbon monoxide is directed at a Ni(111) single crystal. The nickel surface is housed in a UHV chamber with a typical base pressure of less than $10^{-9}$ Torr. After leaving the Ni(111) surface, gas-phase CO is state-selectively ionized by a focused UV laser beam incident at 90° to the molecular beam. The resultant ions are then accelerated into a time-of-flight (TOF) mass spectrometer and detected by two channel electron multiplier arrays (CEMA) oriented in the Chevron configuration. The resultant charge is detected by a gated integrator and stored for later processing on a minior microcomputer.

### A. The Ni(111) surface

The Ni(111) single crystals used in this experiment were commercially available (Aremco). Their stated purity was 99.995%. They were aligned, cut, and polished to within 0.5° of the (111) direction by the manufacturer. The nickel crystals were cleaned *in situ* by repeated $Ar^+$ sputter and anneal cycles. The surface temperature was monitored with two chromel–alumel thermocouples wedged between the face of the nickel sample and the restraining cap. The accuracy of the thermocouples (at high temperatures) was verified using two different optical pyrometers. The surface was heated by electron bombardment of the rear of the sample holder, and the temperature was regulated by a commercial PID controller (Omega). The elemental composition of the near-surface region could be monitored using Auger electron spectroscopy. The chamber was equipped with a grazing incidence electron gun and retarding field electron analyzer (Varian) for this purpose.

Because of the relatively high surface temperatures involved in this study, the major surface contaminant was sulfur that diffused to the surface from the bulk. The near-surface region was depleted of S by very slow sputtering (300 eV $Ar^+$) at 1075 K for many hours. This process had to be repeated every few months. On a more regular basis, the surface was typically simultaneously sputtered and annealed at 1075 K with 400–500 eV $Ar^+$ ions until a clean Auger spectrum was obtained.

### B. The molecular beam source

Ideally, gas/surface scattering experiments should be performed with a translationally monoenergetic source of molecules in the rovibrational ground state. Although such a source of CO molecules is not experimentally feasible at this time, a supersonic molecular beam provides a reasonable approximation of this ideal.

Supersonic beams of CO were produced by expanding a gas mixture from a stagnation pressure of 90 psi through a 400 $\mu$m orifice in a pulsed, solenoid-driven valve (General Valve) operating at 10 Hz (the maximum repetition rate of the Nd:YAG laser). The resulting beam passed through the aperture of a skimmer (Beam Dynamics) approximately 1 cm downstream from the nozzle and into the first buffer chamber. A portion of this beam was selected by a chopper rotating at ~250 Hz. The chopper was composed of a 4.5 in. diameter Al disk with two diametrically opposed 0.030 in. machined slits mounted on the shaft of an AC synchronous motor (TRW Globe). The phase of the motor was monitored with a LED/phototransistor pair, and this signal was used to generate the appropriate delays for the subsequent firing of the pulsed nozzle and laser.

The final molecular beam pulse at the crystal surface was approximately 4 mm in diameter and less than 20 $\mu$s in duration. Although a molecular beam is a very intense source, this short temporal width had one very important effect—*each pulse of gas corresponded to a total dose of ~0.1% of a monolayer.* All of the experiments were performed at surface temperatures of 575 K and above. At these surface temperatures, the residence time of CO on the surface ($\tau$) was short enough to ensure that all trapped molecules desorbed before the next pulse of gas (i.e., $\tau \ll 100$ ms). All results thus apply to the dilute CO coverage limit, and CO–CO interactions could be neglected.

The final translational energy of the molecular beam was controlled by seeding in either $H_2$ or He, and measured using time-of-flight techniques.[10] In our analysis, we assumed that the measured velocity distributions could be expressed in the form

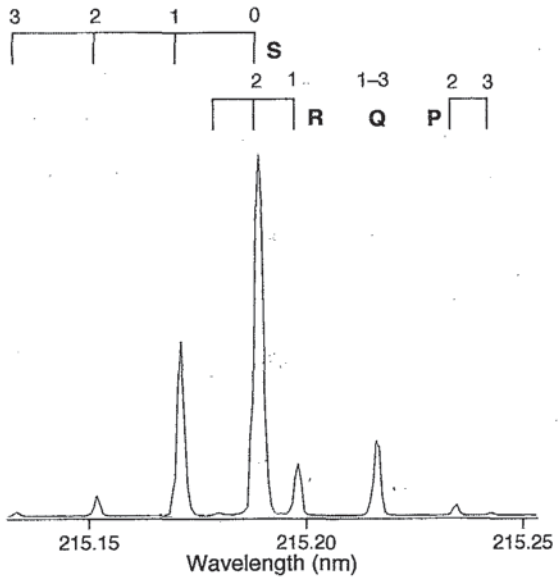


FIG. 2. (2+1) REMPI spectrum of the supersonic nozzle beam of CO via the $E\,^1\Pi$–$X\,^1\Sigma^+$ (0,0) transition. This spectrum is adequately represented by a 5 K rotational temperature.

$$f(v) \propto v^3 \exp[-(v-v_0)^2\alpha^2], \tag{1}$$

where $v_0$ is the streaming velocity and $\alpha$ is the width parameter. The width of the velocity distribution could then be expressed in terms of the dimensionless speed ratio $\sigma$, which was given by

$$\sigma = \frac{v_0}{\alpha}. \tag{2}$$

Given this result, the observed time-of-flight distribution should be given by the convolution of Eq. (1) (under the appropriate change of variables) with the chopper shutter function.

In these experiments, gas mixtures that were 5%–20% CO were used, resulting in translational energies of 0.26–0.45 eV. A few experiments were performed using a neat beam of CO that had a translational energy of 0.09 eV. The speed ratio for the hydrogen expansions was measured to be 18 (irrespective of dilution), while the speed ratio for the helium expansions was 20.

The rotational state distribution of the molecular beam could also be monitored (see Sec. II C). A typical spectrum is shown in Fig. 2. Although such an expansion was not well described by a Boltzmann distribution, the observed rotational population in the first four rotational levels corresponded to a rotational temperature of approximately 5 K.

Since this experiment was very sensitive to contamination, all of the gases used (CO, $H_2$, and He) were of greater than 99.99% purity as quoted by the manufacturer. Unfortunately, CO is subject to contamination by iron pentacarbonyl [$Fe(CO)_5$], when stored at high pressure in a steel container.[11] This contamination was removed by passing CO over an activated charcoal trap (Balston). Without the trap in place, photoionization of the molecular beam

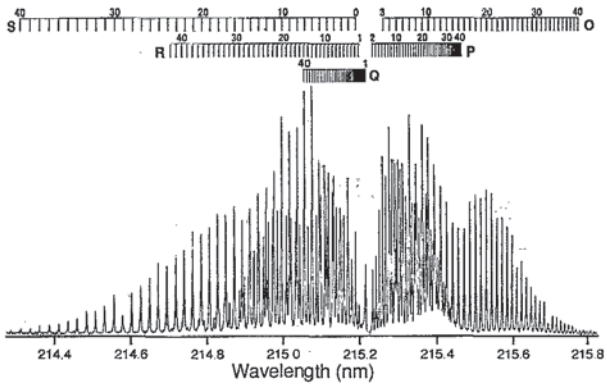


FIG. 3. A typical (2+1) REMPI spectrum via the $E\,^1\Pi$–$X\,^1\Sigma^+$ transition of CO scattered from a Ni(111) surface.

($\lambda \approx 215$ nm) resulted in a strong ion signal with a mass-to-charge ratio of 56 which was attributed to $Fe^+$ formed in the photodissociation of $Fe(CO)_5$. This signal was never observed with the trap in place, nor was any iron contamination of the Ni(111) crystal ever observed.

### C. CO detection

CO molecules were state selectively detected 1 cm from the crystal surface using (2+1) resonance-enhanced multiphoton ionization (REMPI) via either the $E\,^1\Pi$–$X\,^1\Sigma^+$ transition[12] or the $B\,^1\Sigma^+$–$X\,^1\Sigma^+$ transition.[13] Both transitions were accessible with the same Nd:YAG (Quantel 581 C) pumped dye laser system (visible bandwidth $\geqslant 0.55$ cm$^{-1}$). The $E\,^1\Pi$–$X\,^1\Sigma^+$ transition required UV light of approximately 215 nm. To produce radiation of this wavelength, the dye laser was pumped at 532 nm ($2\omega$ of Nd:YAG) and operated at $\approx$645 nm. The output of the dye laser was first doubled in KD*P and then mixed with the residual fundamental in $\beta$-$BaB_2O_4$ (BBO) to effect a net tripling. This scheme typically produced between 2 and 3 mJ of tunable light near 215 nm.

The transition through the $E\,^1\Pi$ state was preferred because all $J$ states were resolved in the spectrum and because it was experimentally more tractable. Unfortunately, this scheme may undercount high-$J$ states because of the effects of rotational predissociation. To minimize undercounting, populations of high-$J$ states ($J \geqslant 15$) were determined only from the $O$ and $P$ branches of the $E$ state. With this exception, the ground state populations were extracted in a manner described previously.[12] A typical $E$ state REMPI spectrum of CO scattered from a Ni(111) surface is shown in Fig. 3.

The $B\,^1\Sigma^+$–$X\,^1\Sigma^+$ transition required UV light of approximately 230 nm. To produce this wavelength, the dye laser was pumped at 355 nm ($3\omega$ of Nd:YAG) and operated at $\approx$460 nm. Although this is an aesthetically pleasing wavelength, the lifetime of the dye is unpleasantly short ($\approx$3–4 h). The output of the dye laser was doubled in BBO to produce approximately 0.5 mJ at the requisite wavelength. A typical $B$ state REMPI spectrum of CO scattered from a Ni(111) surface is shown in Fig. 4. The

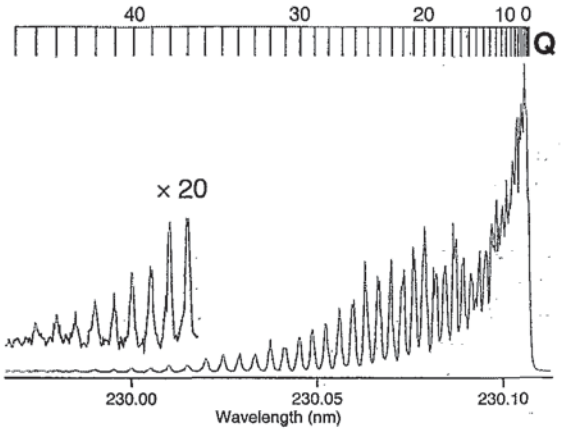


FIG. 4. A typical (2+1) REMPI spectrum via the $B\,^1\Sigma^+$–$X\,^1\Sigma^+$ transition of CO scattered from a Ni(111) surface. The high-$J$ region has been expanded by a factor of 20 for clarity.

spectrum is characterized by a strong $Q$ branch and very weak (but observable) $O$ and $S$ branches. Only the members of the $Q$ branch were used to derive populations, so the populations of low-$J$ states ($J \lesssim 13$) could not be measured with this transition. To extract populations from this spectrum, we first performed a nonlinear Gaussian fit to all resolved and partially resolved peaks using a fixed linewidth derived from the resolved portion of the spectrum. We then extracted the total signal from each transition from the fit. Because the $O$ and $S$ branches of this ($\Sigma$–$\Sigma$)two-photon transition are very weak, we neglected contributions from the perpendicular transition dipole moment. Within this approximation, the two-photon line strengths are independent of $J$,[14] and the ground-state populations should be directly proportional to the measured signal.

To test the validity of this assumption, we measured the REMPI spectrum of a room temperature sample of CO and from this determined the ground rotational state distribution. The results of this measurement are shown in Fig. 5. In this figure, the data are presented in a so-called Boltzmann plot {i.e., ln[population/$(2J+1)$] vs rotational energy}. In this format, an equilibrium distribution falls on a straight line and a rotational temperature can be derived

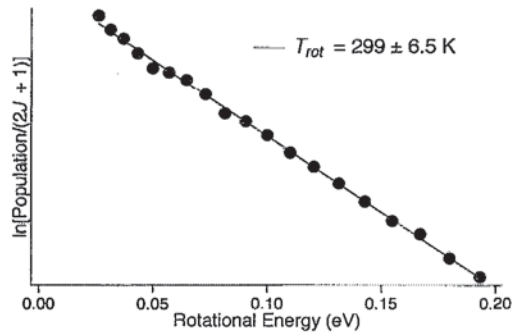


FIG. 5. Rotational populations derived from a $B\,^1\Sigma^+$–$X\,^1\Sigma^+$ REMPI spectrum of a room-temperature sample of CO at a pressure of $1\times10^{-7}$ Torr. The solid line represents the best fit to a Boltzmann distribution.

from the slope of such a plot. Indeed, the measured rotational temperature of 299±6.5 K is in good agreement with the actual temperature.

(2+1) REMPI through the $B\,^1\Sigma^+$ state is slightly more quantitative than the $E\,^1\Pi$ state scheme. For this reason, all of our reported rotational temperatures, with the exception of those reported in Table I, were measured with the $B\,^1\Sigma^+$–$X\,^1\Sigma^+$ transition. Note, however, that under very low laser intensities, a drop in intensity between $J=37$ and $J=38$ is observed. This drop is caused by predissociation of the $B$ state.[13] This problem is more severe in the $v=1$ level—we observed a sharp falloff in intensity above $J=18$ and attribute this decrease to rapid predissociation. Thus the higher-$J$ states of the $v=1$ level were undetectable in this experiment.

In our measurements, no attempt was made to correct for possible rotational polarization effects in the $E\,^1\Pi$–$X\,^1\Sigma^+$ spectrum. The $B\,^1\Sigma^+$–$X\,^1\Sigma^+$ spectrum is insensitive to these effects. We have not corrected for the velocity of the CO molecules, so the reported rotational state distributions are a measure of the final density of CO not the final flux.

The angular dependence of the internal state distribution of CO molecules could be measured by moving the focus of the laser about the surface normal. Experimentally, this movement was accomplished with two orthogonal translation stages on the final turning optics and a rotatable lens [outside the ultrahigh vacuum (UHV) chamber]. The effective in-plane angular resolution was calculated to be $<10°$ ($2\sigma$) along the surface normal and less in other geometries. After the molecules were photoionized, the resulting ions were accelerated into a fixed-position, field-free drift tube used as a time-of-flight mass spectrometer. Because the detector was fixed in space, we were not able to make *quantitative* comparisons of the total flux at different angles.

## III. RESULTS

### A. Surface temperature dependence of residence time

Previous researchers[3] have shown that under our experimentally accessible conditions, no more than 50% of an incident CO beam scatters from a Ni(111) surface. The rest of the incident flux sticks to the surface and later desorbs. The time scale for desorption is determined by the surface temperature, which places a lower limit on the surface temperature studied in this experiment. If the characteristic time scale for desorption approaches or exceeds 100 ms, the repetition time of the experiment, CO builds up on the surface with time. The surface residence time of adsorbed CO molecules can be monitored directly by examining the CO flux in time.

Figure 6 shows temporal distributions of a (pulsed and chopped) 0.36 eV beam of CO after interaction with the Ni(111) surface as a function of surface temperature. These data were obtained by measuring the population in a blended line ($J=7$ and 15) along the specular direction ($\theta_{inc}=30°$) as a function of the delay between the opening

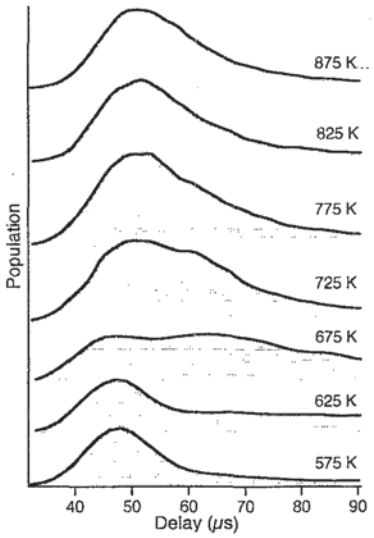


FIG. 6. The temporal distribution of CO leaving a Ni(111) surface along the specular direction as a function of surface temperature. The incident CO pulse was approximately 20 $\mu$s in duration. The incident translational energy was 0.36 eV, the incident angle was 30°, and the zero time is arbitrary.

of the pulsed nozzle and the subsequent firing of the laser. In this plot, the data were smoothed using a five-point binomial filter.[15] At the lowest surface temperature, 575 K, the temporal distribution is similar to that of the incident beam. This peak results predominantly from molecules that have scattered from the surface. Both desorbing molecules and scattered molecules that have undergone collisions with the walls of the chamber contribute to the small tail that occurs at long times. As the surface temperature is raised to 675 K, the tail increases in intensity (i.e., moves to shorter delay times) owing to the decreased residence time of adsorbed molecules. Finally, at 875 K, the scattered and desorbed pulse shapes show little difference.

This effect could be used to our advantage. At 575–625 K, the surface temperature is just cold enough to effectively discriminate against the trapped molecules, and hence warm enough to ensure that all of the trapped molecules had desorbed before the next laser shot. The validity of this assumption is further supported by calculations of the surface residence time (half-life) based on the kinetic parameters of the CO/Ni(111) system reported by Miller *et al.*[5] At 575 K, the surface residence time is calculated to be 5 ms or 20 half-lives between laser shots.

Note that this technique only *discriminates* against trapping/desorption; it does not entirely remove this channel. Under conditions unfavorable for scattering, such as low incident beam energy or far subspecular detection, a significant amount of the observed CO could come from desorption. Similarly, at long time delays ($>20$ $\mu$s after the beginning of the pulse), a transient background signal occurs from scattered molecules interacting with the walls of the chamber.

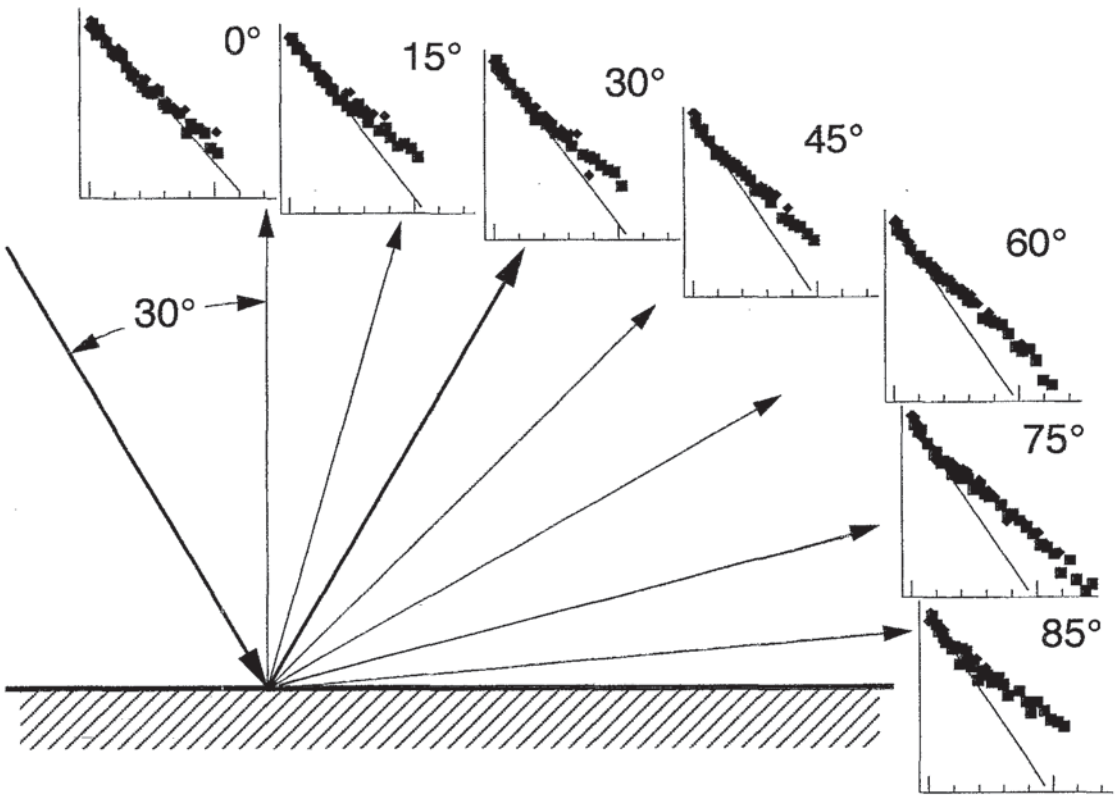


FIG. 7. The angular dependence of the rotational state distribution of CO scattered and desorbed from a Ni(111) surface. The incident translational energy was 0.36 eV, the incident angle was 30°, and the surface temperature was 875 K. The data are presented in Boltzmann plots {i.e., ln[population/$(2J+1)$] vs rotational energy} and the minor ticks correspond to 0.06 eV. The relative intensities have been normalized. The straight lines indicate the initial slope of the rotational distribution (see the text).

TABLE I. Parameters describing the angular dependence of the rotational state distribution of CO scattered and desorbed from a Ni(111) surface. These data describe the rotational distributions pictured in Fig. 7. The average rotational energy $\langle E_{rot}\rangle$ and the standard deviation of the rotational energy distribution $\sigma(E_{rot})$ were derived from the entire distribution, while the low-$J$ rotational temperature, $T_{rot}$ was derived from $0<J<15$.

| $\theta_{scat}$ | $\langle E_{rot}\rangle$ cm | $\sigma(E_{rot})$ cm$^{-1}$ | $T_{rot}(J<15)$ K |
|---|---|---|---|
| 0° | 540 | 8.6 | 710 |
| 15 | 560 | 8.4 | 610 |
| 30 | 580 | 9.2 | 610 |
| 45 | 560 | 9.5 | 540 |
| 60 | 600 | 9.5 | 550 |
| 75 | 620 | 9.8 | 530 |
| 85 | 620 | 9.9 | 540 |

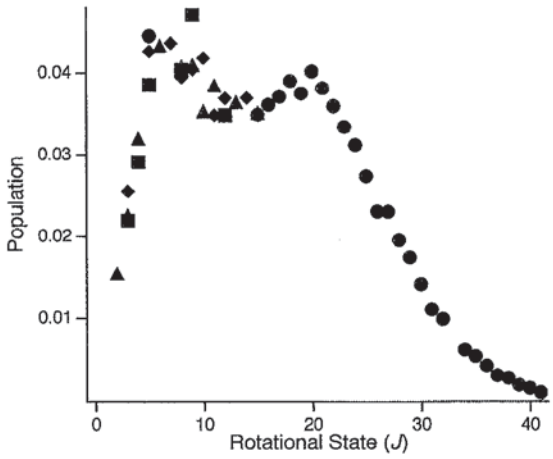


FIG. 8. Rotational state distribution (normalized to unity) of CO molecules scattered to the far superspecular. These data were obtained at $E_{inc}=0.36$ eV, $T_s=625$ K, $\theta_{inc}=30°$, and $\theta_{scat}=75°$. The populations were determined from the $O$ (circles), $P$ (triangles), $R$ (diamonds), and $S$ (squares) branches.

## B. Angular dependence of rotational distributions

Figure 7 illustrates the angular dependence of the rotational state distribution of CO molecules scattered and desorbed from a 725 K Ni(111) surface. In this experiment, the 0.36 eV beam of CO was incident at a 30° angle to the surface normal, and a rotational distribution was obtained at each final angle shown. Because the relative fluxes could not be measured, the final state populations at each angle were normalized to unity. The distributions are presented in Boltzmann plots with identical scaling factors. The tick marks on the abscissa are 0.06 eV apart. The straight lines are solely for illustrative purposes and represent the best fit straight line to all rotational states below 0.06 eV (i.e., $0<J<15$). Over this small region, all of the distributions appear straight; however, *we do not mean to imply that this region of the distributions is the result of an equilibrium process.* The inverse slope of these lines in units of degrees Kelvin is tabulated in Table I.

That the rotational state distribution is sensitive to the final angle is immediately apparent. Molecules leaving the surface along the surface normal have a rotational distribution that is well fit by a Boltzmann distribution; however, molecules leaving at other angles are clearly non-Boltzmann. Additionally, the functional form of the distributions appears to change with angle. The highest rotational states are seen in the far superspecular—here, 45° past the specular angle.

To further study the differences in these distributions, a method for quantifying these distributions must be adopted. We have chosen to use the average rotational energy $\langle E_{rot}\rangle$ and the standard deviation of this quantity $\sigma(E_{rot})$. Table I lists these quantities for the data in Fig. 7. Note that the average rotational energy increases almost monotonically with angle from the surface normal. The width of the distribution also increases with final angle.

## C. Far superspecular scattering

Because Fig. 7 indicates that the most "dramatic" rotational distributions occur in the far superspecular direction, we have examined this region in some detail. Figure 8 shows the rotational state distribution of molecules scattered to the far superspecular—45° past the specular direction. These data were obtained with a 0.36 eV beam of CO incident 30° from the surface normal and with the surface temperature held at 625 K. This temperature is sufficiently low to discriminate against the trapping/desorption channel.

Two points are apparent from this distribution. First, the distribution is clearly *bimodal* and hence cannot be ascribed to an equilibrium process. Second, very high rotational states are populated in this process. For CO, $J=40$ corresponds to 0.39 eV of rotational energy. This energy is slightly greater than the nominal translational energy of the molecular beam and 30% higher than the normal component of the beam energy (i.e., the energy associated with momentum normal to the surface).

To determine the source of this large rotational excitation, we have examined the effect of incident translational energy on the final rotational state distribution. Figure 9 shows the rotational state distribution of molecules with three different incident translational energies. The incident angle, final angle, and surface temperature for this data are the same as in Fig. 8. We have chosen, however, to display this data in a Boltzmann plot to emphasize the high-$J$ region. In this format, the bimodality seen in Fig. 8 appears as a "kink" in the distribution. Figure 9 shows that the position of this kink is energy dependent; as the incident translational energy of the molecular beam is increased, the kink moves to higher rotational energies. A more subtle, but clearly visible point is that the slope of the linear, low-$J$ region (see Fig. 7) is also dependent on beam energy.

The total incident energy of the molecular beam is plotted at the bottom of Fig. 9. These data were obtained with the molecular beam at a 30° angle from the surface normal, so the normal component of the translational energy would be 75% of the quantity displayed. To a good approximation, the highest observed rotational state is given by the *total incident energy* of the molecular beam.

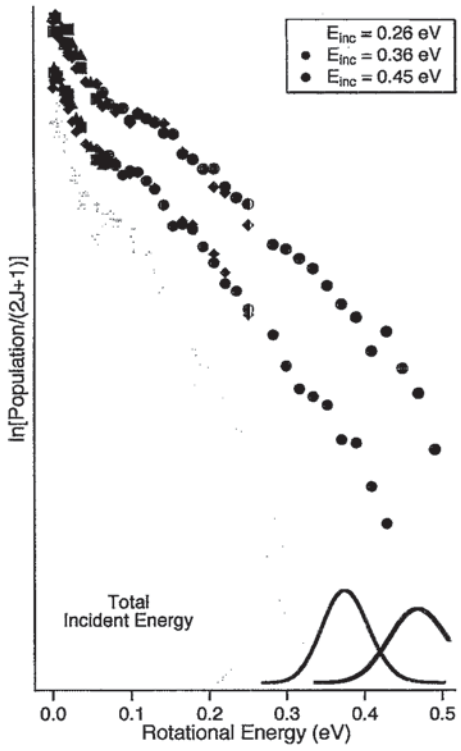


FIG. 9. Boltzmann plots showing the variation of rotational excitation of molecules scattered to the far superspecular ($\theta_{inc}=30°$ and $\theta_{scat}=75°$) with translational energy. The three distributions have mean energies of 0.26 (light gray), 0.36 (dark gray), and 0.45 eV (black). The measured translational energies are displayed at the bottom for comparison. The symbols are the same as in Fig. 8.

### D. Surface temperature dependence of rotational distributions

We studied the surface temperature dependence of two representative regions of the angular distribution—the near-normal region and the far superspecular region.

#### *1. Near-normal detection*

In lieu of examining the flux exactly along the normal direction, we chose to look 10° away from the normal in the subspecular direction. This geometry was 40° from the specular direction and was chosen to minimize the contribution from scattered molecules. To further discriminate against scattering, the data were obtained with an incident translational energy of 0.09 eV. Tang *et al.*[3] have shown that at this energy, only 15% of the incident molecular beam scatters from the surface.

Figure 10 is a Boltzmann plot of the rotational state distribution of molecules observed in the near-normal direction at two different surface temperatures. Along this direction, surface temperature and rotational excitation appear to be strongly coupled; an increase in the surface temperature leads to an increase in the amount of rotational excitation. Additionally, both distributions appear to be linear in this format and curvature is not apparent. Because of this behavior, we have chosen to parametrize these distributions in terms of a "rotational temperature" obtained from the slope of these curves.

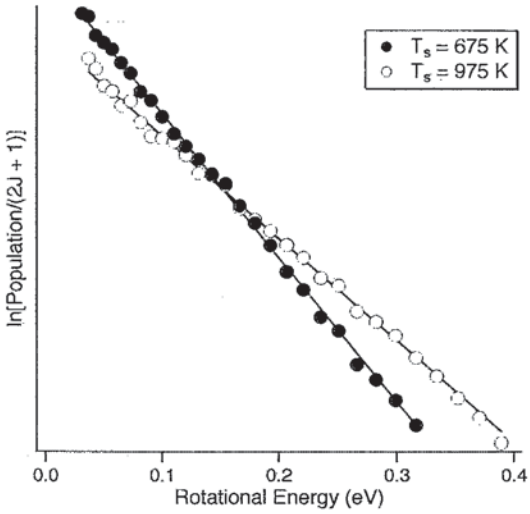


FIG. 10. The Boltzmann plot of the rotational distribution of CO desorbed from a Ni(111) surface at two different surface temperatures. The data were acquired with $E_{inc}=0.09$ eV, $\theta_{inc}=30°$, and $\theta_{scat}=-10°$. The solid circles represent data acquired at $T_s=675$ K and the open circles represent those acquired at $T_s=975$ K. The lines are linear least-squares fits to the data.

Figure 11 shows the relationship between the measured rotational temperature of molecules observed in the near normal direction as a function of surface temperature. The heavy solid line is the best fit to all points with $T_s \geq 675$ K. Over this range, the observed rotational temperature is $0.82 \pm 0.08$ (95% confidence limit) of the surface temperature. The data acquired at the lowest two surface temperatures deviate from this line. At these temperatures, the experiment began to discriminate against the trapping/desorption channel, and as expected, the sig-

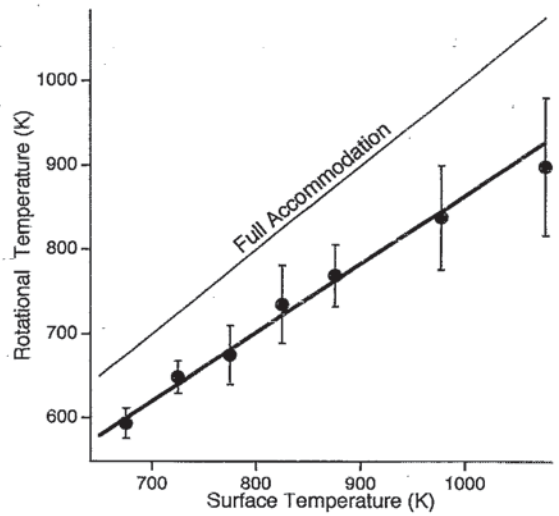


FIG. 11. Rotational temperature of CO desorbing from a Ni(111) surface as a function of surface temperature. The heavy line is the best fit to all points with $T_s \geq 675$ K, the thin line corresponds to complete rotational accommodation, and the error bars are 95% confidence limits based on four measurements.

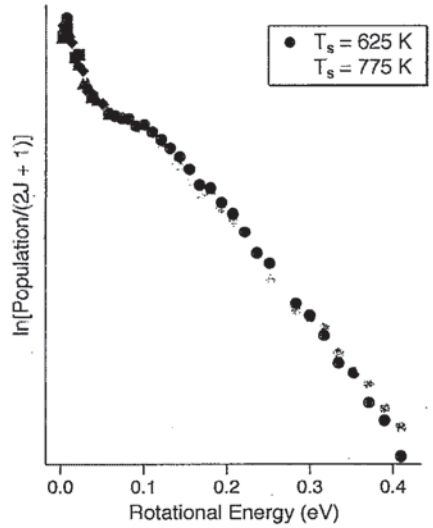


FIG. 12. The Boltzmann plot of the rotational distributions of molecules scattered to the far superspecular at two surface temperatures with $E_{inc}$ =0.36 eV, $\theta_{inc}$=30°, and $\theta_{scat}$=75°. The black points correspond to $T_s$ =625 K and the gray points correspond to $T_s$=775 K. The two distributions have been normalized to the same total population. The symbols are the same as in Fig. 8.

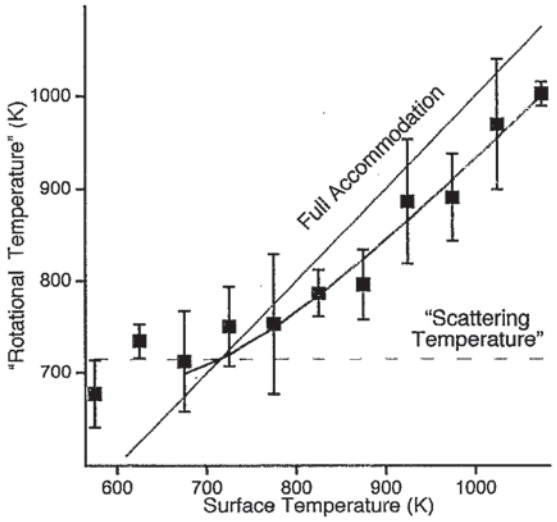


FIG. 13. Rotational temperature (see the text) of CO detected in the superspecular as a function of surface temperature with $E_{inc}$=0.36 eV, $\theta_{inc}$=30°, and $\theta_{scat}$=60°. The heavy line is the best fit (see the text) and the dashed line indicates the best fit "scattering temperature." The light line represents complete rotational accommodation and the error bars are 95% confidence limits based on four measurements.

nal fell sharply. The flux measured at these temperatures arises from the weak scattering channel.

### 2. Far superspecular detection

As discussed previously, the most "non-Boltzmann" rotational distributions were observed in the far superspecular direction. Consequently, this geometry was chosen as the second representative one for study. In these experiments, the molecular beam was incident at a 30° angle from the surface normal and the detection angle was 75°. Figure 12 shows a Boltzmann plot of the rotational distribution of molecules observed in far superspecular direction at two different surface temperatures $T_s$=625 and 775 K. Over this range, the distributions do not differ dramatically. At the higher surface temperature, the rainbow feature appears to be somewhat blurred, and it is possible that the high-$J$ tail of this distribution has a somewhat greater slope. Of course, this comparison is not completely fair, since at the lower surface temperature, the experiment discriminated against the trapping/desorption channel.

To understand this small surface temperature dependence, the observed distributions must first be quantified in some fashion. As can be seen in Fig. 12, these distributions are clearly non-Boltzmann; however, the high-$J$ tail appears linear on a Boltzmann plot. Because of this linearity, we have chosen to fit the high-$J$ region (i.e., all $J$'s$\geqslant$ 25, $E_{rot}\geqslant$ 0.15 eV) to an apparent "rotational temperature." In doing so, we do not mean to suggest that this portion of the distribution reflects an equilibrium distribution—we simply use this as a convenient parametrization.

Figure 13 shows the dependence of this high-$J$ rotational temperature on the surface temperature. At low surface temperatures, the slope of the high-$J$ tail is relatively insensitive to the surface temperature, while at higher temperatures, it appears to track the surface temperature.

Because both the normal and superspecular rotational distributions display similar surface temperature dependencies at temperatures above $T_s\approx$850 K, we now consider the possibility that all of the surface temperature dependence in the far superspecular direction (Fig. 13) is caused by the trapping/desorption channel. Molecules leaving the surface along the surface normal are primarily from the trapping/desorption channel; however, earlier studies by Steinrück, Winkler, and Rendulic[4] have shown that CO desorbs from Ni(111) in a broad, cos $\theta$ angular distribution. Thus, contributions from trapping/desorption occur at all angles.

If all of the surface temperature dependence is caused by contributions from the trapping desorption channel, the observed rotational distributions would be composed of two parts as illustrated in Fig. 14. The black points represent the (assumed temperature independent) contribution from the scattering channel, whereas the gray lines represent the contribution from desorption at three different surface temperatures. We have assumed that the relative amount of trapping/desorption remained constant with temperature, so the areas under the three gray distributions are identical. The key point is that the fraction of desorbing molecules with $J\geqslant$25 *increases with surface temperature* because the average energy of the trapping/desorption channel increases with surface temperature. Recall that only these high-$J$ states were included in the experimental measurement shown in Fig. 13.

If these assumptions are valid, the total population (with $J\geqslant$25) $P(J)$ should be given by

$$P(J)=(2J+1)\{\exp[-E_{rot}(J)/kT_{scat}] + \alpha\exp[-E_{rot}(J)/\beta kT_s]\}, \quad (3)$$

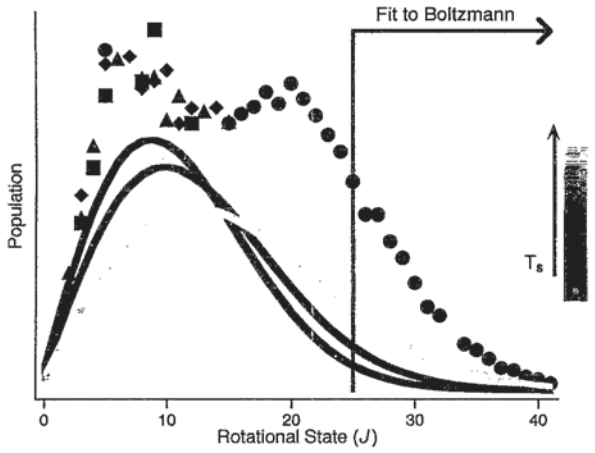


FIG. 14. A schematic of the assumed surface temperature dependence of CO in the superspecular direction. The black data points represent the contribution from scattering; the gray lines represent the contribution from desorption at three surface temperatures $T_s$=575, 725, and 1075 K. The symbols are the same as in Fig. 8.

where $E_{\rm rot}(J)$ is the rotational energy, $T_{\rm scat}$ is "scattering temperature" (i.e., the slope of the high-$J$ tail in the absence of trapping/desorption), $\alpha$ is related to the relative amount of trapping/desorption, and $\beta$ controls the deviation of the desorption temperature from the actual surface temperature. From this expression for $P(J)$, an apparent temperature $T_{\rm app}$ can be found by fitting $\ln[P(J)/(2J+1)]$ vs $-E(J)/kT_{\rm app}$ to a line over the range $25 \leqslant J \leqslant 50$.

The scattering temperature $T_{\rm scat}$ could be experimentally measured from the low surface temperature data, where the contribution from trapping/desorption was small. For our analysis, we used the weighted average of data obtained at 575 and 625 K. Assuming that the desorption temperature is independent of scattering angle, we set $\beta=0.82\pm0.08$ from our previous measurements. Using these parameters, Eq. (3) cannot fit the data as presented in Fig. 13. The reason is clear; the rotational temperatures we measured near the surface normal (Fig. 11) are lower than the temperatures in Fig. 13. We could fit our data if we assumed that the desorption temperature was closer to the surface temperature. Values of $\beta$ in the range of 0.95–1.0 resulted in reasonable fits to the data. The heavy line in Fig. 13 is the best fit assuming that $\beta=1.0$.

### E. Vibrational excitation

Vibrationally excited molecules ($v=1$) were observed in the far superspecular direction at all surface temperatures; however, predissociation of the $B\,^1\Sigma^+$ state of CO precluded measurement of rotational states higher than $J=17$.[13] Similarly, congestion in the $E\,^1\Pi$–$X\,^1\Sigma^+$ spectrum prevented detection of all but a few low $J$ transitions. The degree of vibrational excitation was strongly correlated to surface temperature; however, the absence of high $J$ data does not allow us to conclusively attribute the vibrationally excited molecules to the scattered channel.

## IV. DISCUSSION

As shown in the preceding section, the rotational state distribution of CO after interaction with a Ni(111) surface is sensitive to a number of parameters—incident translational energy, detection angle, and surface temperature. Furthermore, these parameters are not independent. In this section, we explain this behavior by considering competition between two channels—scattering and trapping/desorption. We discuss first the far superspecular rotational distributions as they are the most dynamical, and then discuss how the strong angular dependence can be explained in terms of competition between these two channels. Finally, we show that the surface temperature dependence is consistent with this picture.

### A. Far superspecular scattering

Three important characteristics of the rotational state distributions are observed in the far superspecular direction. First, as shown in Figs. 8 and 9, these distributions are clearly non-Boltzmann; in fact, they are bimodal. Second, the features in these distributions (i.e., the positions of the extrema) are dependent on the incident translational energy of the CO molecules. Third, very high rotational states are populated; the highest observed rotational energy is well matched to the total incident energy of the molecular beam.

Of these observations, the most important is the strong translational energy dependence. Molecules that trap on the surface and later desorb will not be influenced by incident beam parameters. Because of this, we believe that the scattering channel predominates in the far superspecular direction. Although trapping/desorption may be nonnegligible at this angle under some conditions (e.g., high surface temperatures), any features that are dependent on incident energy must be attributed to scattering.

#### *1. Rotational rainbow*

The bimodal rotational distribution depicted in Fig. 8 is characteristic of a *rotational rainbow*.[2] A rotational rainbow in gas/surface scattering was first seen by Kleyn, Luntz, and Auerbach[16] in the scattering of NO from Ag(111). Unlike the CO/Ni(111) system, NO/Ag(111) is a very weakly interacting system with a binding energy of $\leqslant 0.2$ eV.[17] Subsequent to the Kleyn *et al.* work, other investigators found a number of weakly interacting systems that display rotational rainbows. Prior to our work, no clear evidence has been presented of a rotational rainbow in a strongly chemisorptive system, although a number of such systems have been studied.[18]

Rotational rainbows are perhaps most easily understood by analogy with the "scattering" of an (American) football from a flat surface. When a football hits a surface, the final rotational state is determined by the impulsive torque and hence by $\gamma$, the angle the long axis of the football makes with the surface. If the football hits the surface end on ($\gamma=0°$ or 180°) or side on ($\gamma=90°$), there is no torque in the collision and the football leaves the surface nonrotating. If the football hits at any other angle, there is a torque and the football leaves the surface rotating. At

some specific impact angle, typically $\gamma \approx 35°$, the football experiences maximum torque and scatters into $J_{max}$, the highest accessible rotational state for a given translational energy and incident angle. This special angle $\gamma$ corresponds to a singularity in the differential cross section, and so classically the population at $J_{max}$ is divergent.

In general, the term *rainbow* is used to denote a singularity in a differential scattering measurement.[19] The familiar optical rainbow is caused by the scattering of light into a preferential final angle by small water droplets.[20] A rotational rainbow is due to the scattering of particles into a preferential final rotational state $J_{max}$. Although both phenomena correspond to classical singularities, these are, of course, not observed in reality. Instead, an optical rainbow appears as a bright region in the sky, and a rotational rainbow appears as a "bump" in the rotational distribution. In Fig. 8, the rotational rainbow is observed at $J \approx 20$.

The actual value of $J_{max}$ is dependent on a number of parameters. In a simple impulsive system (such as a real football scattering from a surface), $J_{max}$ is dependent on the shape of the particle (e.g., round particles never experience a torque) and its incident translational energy. If the surface is flat and frictionless, only the component of the particle's incident momentum that is *normal to the surface* is coupled into rotation. In this case, the system is said to display *normal energy scaling.* If the surface is either corrugated or frictional, then both the parallel and perpendicular components of the particle's momentum may contribute to the applied torque.

This translational energy dependence provides a key test for the assignment of a rotational rainbow. A true rainbow moves to a higher rotational energy as the incident translational energy increases. Note that by itself, the observation of a non-Boltzmann rotational distribution does not establish the presence of a rotational rainbow. For example, a distribution that is the sum of two different Boltzmann distributions (at different characteristic temperatures) appears non-Boltzmann, even though both component distributions are Boltzmann. Figure 9 shows that the rotational energy of the "kinks" in the CO/Ni(111) rotational distribution is dependent on the incident translational energy; thus these features originate from dynamical processes.

At this point we should note that whereas a symmetric particle, such as a football or a $N_2$ molecule, displays a single rotational rainbow, an asymmetric particle will have more than one rainbow. For example, because the center of mass of CO is not equidistant between the two nuclei, a C-end down collision must feel a different torque than the corresponding O-end down collision. Because of this difference, the scattering of a heteronuclear diatomic molecule from a surface should lead to (at least) two rainbows—each rainbow corresponding to the interaction of a different end of the molecule with the surface. Of course, the separation between the two rainbows is governed by the anisotropy of the potential and may or may not be observable. Recent measurements by Rettner, Kimman, and Auerbach[21] indicate that this splitting is too small to be observed in the scattering of NO from Ag(111).

As noted in the Introduction, the CO/Ni(111) potential is quite anisotropic, and so it would be difficult to argue that the two rainbows are closely spaced and hence unresolvable. Nevertheless, our rotational distributions show no hint of the expected second rainbow. This observation raises two questions. First, is the observed rainbow caused by the interaction of the C end or O end of the molecule with the surface? Second, what happened to the other rainbow? The remainder of this section will endeavor to answer the first question and the next section, the second.

Our description of rainbow scattering is so far incomplete because we have neglected the effect of the attractive part of the potential. The position of the rainbow may be affected by an attractive potential in two ways. The first is relatively straightforward—the attractive potential accelerates the particle into the surface, thereby increasing its translational energy during the collision with the repulsive wall. Lykke and Kay[22] observed this effect in the scattering of $N_2$ from Au(111)—a system with a binding energy estimated to be 0.17 eV. This effect should be somewhat more complicated in the scattering of CO from Ni(111), as the attractive potential is markedly different for the two ends of the molecule. Molecules incident on the surface C end down should feel a much stronger acceleration than ones incident O end down, so this effect should further separate the two rainbows.

If the attractive potential is orientationally anisotropic, $J_{max}$ is also affected in another way. The force felt by a molecule in a given orientation is determined by the gradient of the potential at that point. It follows that any orientational anisotropy in the potential leads to a torque on the molecule and hence a change in the final angular momentum. This effect is clearly seen in the classical trajectory calculations of Muhlhausen, Williams, and Tully[23] on the scattering of NO from transition metal surfaces. In these calculations, as on most transition metal surfaces, the N end of NO is much more strongly attracted to the metal surface than the O end. Because of this difference, when the molecule is incident on the surface in an unfavorable orientation, it feels a strong "reorientation force" toward the N-end down configuration. If the molecule does not stick to the surface (as is true for most trajectories in this calculation), the effects of this torque are reflected in the final rotational state of the molecule as it scatters from the surface.

Given that all of these considerations may affect the position of the rotational rainbows, determining the identity of the observed CO/Ni(111) rainbow would at first seem impossible. Instead of arguing where the C-end and O-end rainbows *should* appear, we take a different tack. We will compare our rainbow with a similar, previously identified rainbow. Fortunately, the CO/Ni(111) rainbow is in approximately the same position as the one observed by Sitz *et al.*[24] in the scattering of $N_2$ from Ag(111). For a 0.3 eV beam of $N_2$ incident at 30°, the $N_2$/Ag(111) rainbow appears at $J \approx 17$ ($E_{rot} = 0.073$ eV), whereas at the same incidence angle, we observe maxima at $J \approx 18$ ($E_{rot}$

$=0.078$ eV) for $E_{inc}=0.26$ eV and at $J\approx 20$ ($E_{rot}=0.096$ eV) for $E_{inc}=0.36$ eV. The similar rainbow energies are interesting because not only do CO and $N_2$ have the same mass, they are also isoelectronic. Additionally, the reduced masses of CO and Ni are not too different from the reduced masses of $N_2$ and Ag, although the masses of Ni and Ag are different. This observation implies that *the observed CO/Ni(111) rainbow comes from a part of the interaction potential that is similar to the $N_2$/Ag(111) potential.*

The interaction of $N_2$ with Ag(111) is a very weak one; the well depth in this system has been estimated to be only 0.07 eV.[25] In a combined experiment and classical trajectory simulation, Kummel *et al.*[25] have shown that this system can be modeled qualitatively by an ellipsoid hitting a somewhat corrugated surface. From this line of thought, we conclude that *the observed CO/Ni(111) rainbow is caused by the O end of CO hitting the surface.* The fact that the rainbow in this system is approximately 15% higher in energy than the one observed in the $N_2$/Ag(111) system can likely be attributed to a stronger interaction between the O end of CO and Ni(111) than between (the N end of) $N_2$ and Ag(111).

### 2. Rotational trapping

We now turn to the problem of the "missing" C-end rainbow. Unlike the O end of the molecule, the C end of CO interacts very strongly with the Ni surface. The desorption energy for this configuration is 1.3 eV.[5] If the O-end rainbow is caused by a predominately impulsive interaction with the repulsive potential [as in the scattering of $N_2$ from Ag(111)], the C end of the molecule should experience a similar interaction modified by the strong attractive forces. Because of this reasoning, we would expect the C-end rainbow to appear at (much!) higher rotational energies than the O-end rainbow. As seen in Fig. 9, however, the high-$J$ tail of the rotational distribution is featureless; there is no evidence of a second rainbow. Instead, it appears that all energetically accessible rotational states are populated.

Up to complete translational-to-rotational energy conversion is not a signature of a rotational rainbow; instead, it suggests that an energetic constraint such as *rotational trapping* is affecting the dynamics. The term *rotational trapping* was coined by Polanyi and Wolf[26] and based on their classical simulations of diatomic/surface scattering. Simply put, the acceleration of the molecule into the surface prior to the repulsive collision enhances the translational-to-rotational energy conversion during the impulsive collision. If the attractive well is on the order of (or greater than) the molecule's incident translational energy, some collisions may convert so much linear momentum into rotation that the molecule no longer has enough linear momentum to escape the surface. These molecules become trapped at the surface (at least temporarily). The key parameter here is translational energy, not total energy. If a molecule has enough total energy (rotational +translational) to escape the surface but not enough translational energy, it is said to be rotationally trapped.

We believe rotational trapping accounts for the missing C-end rainbow. In the calculations of Polanyi and Wolf, the collisions that led to rotational trapping were just those that would have led to a rotational rainbow in the absence of a strongly attractive potential. We reach this conclusion because both phenomena are associated with large translational-to-rotational energy transfers. In a weakly attractive system, such as the interaction of the O end of CO with Ni(111), the rotational rainbow occurs at $J_{max}$, the higher populated rotational state. Similarly, in a strongly attractive system, such as the interaction of the C end of CO with Ni(111), rotational trapping occurs for all rotational states higher than the energetic limit (i.e., $E_{rot}\geqslant E_{trans}$). Although there may still be a rainbow, it will be trapped at the surface and not directly observable in the molecules scattered from the surface.

A molecule that is rotationally trapped at the surface does not necessarily remain trapped at the surface for more than a few bounces. Because translational-to-rotational energy conversion is facile, it follows that rotational-to-translational energy conversion must be equally facile. This situation implies that a molecule that scatters into a very high (but trapped) rotational state on its first collision with the surface may be able to kick itself off the surface on a subsequent bounce by converting some rotational energy back into translational energy. On each bounce, however, the molecule may lose energy by exciting phonons; this will limit the number of bounces a molecule can make before escaping. The role of multiple bounces has been examined in calculations by Jacobs and Zare[27] on the NO/Pt(111) system and by Harris and Luntz[28] on the CO/Pt(111) system. In both studies, a significant number of molecules made two to four collisions with the surface before escaping into the gas phase.

Although rotational trapping does not invariably lead to chemisorption, it may be viewed as a "dynamical precursor" to chemisorption. By allowing the molecule to make a number of collisions with the surface prior to scattering into the gas phase, rotational trapping can enhance energy flow from the molecule to the surface and thus increase the sticking coefficient. This reasoning implies that molecules that hit the surface nominally C end down have a higher sticking coefficient than those that hit nominally O end down. Although this prediction has not been directly verified for CO scattering, Kuipers *et al.*[29] and Fecher *et al.*[30] have examined the orientationally resolved sticking coefficients for NO on Pt(111) and Ni(110), respectively. In both cases, molecules initially oriented N end down (i.e., strongly interacting end down) have a higher sticking coefficient than those oriented O end down.

A precursor to molecular chemisorption in the CO/Ni(111) system was suggested by Tang *et al.*[3] to explain the observed translational energy dependence of the sticking coefficient in this system. Subsequent trajectory calculations by Doren and Tully[31] on model potentials showed that these observations can indeed be explained by a rotationally anisotropic interaction potential. Although these calculations were not primarily concerned with the final rotational state distributions of the scattered molecules,

Doren and Tully did note that at translational energies relevant to this study, the scattered component was composed primarily of molecules that arrive at the surface O end down.

The final topic to be considered in this section is the energy of the onset of rotational trapping. As seen in Fig. 9, the energetic cutoff appears to correspond to near complete translational-to-rotational energy conversion (under the conditions of these experiments). Since these experiments were carried out at an incident angle of 30°, the data show that incident momenta both perpendicular and parallel to the surface are converted into rotation. As mentioned previously, the conversion of parallel momentum into rotation implies the presence of in-plane forces; the surface must be corrugated. If the surface were flat and frictionless, momentum parallel to the surface would be conserved in the scattering process and, for an incident angle of 30°, at most 75% of the total incident translational energy could be converted to rotation.

These results are interesting to compare with those from a more weakly interacting system such as NO/Ag(111). Detailed studies of the velocity-resolved angular distributions of NO scattered from Ag(111) by Rettner, Kimman, and Auerbach[21] showed that even in such a weakly interacting system, parallel momentum is only approximately conserved. For example, under conditions similar to our experiments ($E_{inc}=0.47$ eV and $\theta_{inc}=30°$), the average change in parallel momentum was only 10% of the corresponding change in perpendicular momentum.

That the CO/Ni(111) potential is corrugated should not be too surprising. Although the term *corrugation* invokes a picture of a rough, bumpy surface [which is seemingly at odds with the close-packed nature of the Ni(111) surface], it simply means that the surface potential is laterally anisotropic. One manifestation of this corrugation is that CO has preferred binding sites. On a Ni(111) surface, both the bridge and atop sites are populated; these sites differ in energy by about 0.04 eV.[32] There must be even stronger lateral variations in the potential, however, because the activation barrier to diffusion has been measured to be 0.3 eV.[33] Moreover, the activation barrier to diffusion is only a lower limit to the total degree of corrugation because very repulsive regions of the potential may play a small role in diffusion.

### B. Angular dependence of rotational state distribution

The previous discussion makes clear that the far superspecular scattering distribution is dominated by inelastic scattering. We now turn to the more complicated angular dependence of the final rotational state distribution illustrated in Fig. 7. These data were acquired at a surface temperature where both the scattering and trapping/desorption channels contributed to the observed flux.

Molecules leaving the surface along the surface normal had rotational distributions that are well described by a Boltzmann distribution. Although this behavior is characteristic of an equilibrium process (such as trapping desorption), it is not conclusive proof of one. Figures 10 and 11 show that the rotational distributions of molecules leaving the surface in the near-normal direction are strongly correlated with the surface temperature. Additional measurements have shown that the rotational distributions in this direction are insensitive to the incident energy of the molecular beam (over the range 0.09–0.36 eV). These three factors taken together suggest that the observed CO flux in near-normal geometry is caused primarily by trapping desorption.

For all detection angles, the low-$J$ region of the rotational distributions appears to be linear on a Boltzmann plot. Earlier studies by Steinrück *et al.*[4] have shown that the angular distribution of the CO/Ni(111) trapping/desorption channel is remarkably well fit by a $\cos\theta$ form. Hence, at sufficiently high surface temperature, the trapping/desorption channel must make some contribution to the measured flux at all angles. Even at 85° from the surface normal, the trapping/desorption channel would be almost 10% as large as along the surface normal. Because of this contribution, it is tempting to ascribe the low-$J$ "Boltzmann" region at every angle to trapping/desorption; however, this interpretation is problematic. As can be seen in Fig. 7 and in Table I, the slope of the linear, low-$J$ region of the rotational distributions is dependent on the detection angle. This dependence argues against a purely equilibrium process and for a dynamic contribution.

A "pseudo-Boltzmann" low-$J$ rotational distribution can arise from a purely dynamic process. For example, Barker, Kleyn, and Auerbach[34] have shown that scattering from some simple potentials leads to a singularity at zero rotational energy. For this reason, some, but not all, authors also call this low-$J$ feature a rotational rainbow. If a finite number of trajectories are considered, the singularity leads to a linear region in a Boltzmann plot of the final rotational state distribution. In their classical trajectory calculation, Muhlhausen, Williams, and Tully[23] also observed a linear low-$J$ region in the rotational distribution; however, they found that a number of different types of scattered trajectories, including some that had undergone multiple bounces, contributed to this region of rotational excitation. Additionally, Brunner and Brenig[35] have shown that corrugation further complicates the picture. Given these facts, we believe that although there does appear to be a dynamic feature at low $J$ in the rotational distribution, it likely arises from a number of different types of trajectories, perhaps involving both single and multiple collisions with the surface. At some angles, this low-$J$ dynamical contribution is overshadowed by the stronger trapping/desorption channel.

In contrast to the low-$J$ angular distribution, highly rotationally excited molecules are preferentially found in the superspecular direction. For the conditions of Fig. 7, the highest observed rotational states occur in the far superspecular direction—45° past the specular. In contrast, the rotational distributions observed along the specular direction are only slightly non-Boltzmann. Comparing the highest observed rotational states between different scattering conditions can be misleading, though because our ion collection efficiency was a strong function of the exit angle.

A more trustworthy measure is the average rotational energy and first moment of the entire distribution as given in Table I. Here the average rotational energy appears to increase with scattering angle. From these data, $\langle E_{\rm rot} \rangle$ is seen to increase almost monotonically with scattering angle; it is not clear that the highest rotational excitation occurs at 75°.

Preferential scattering of highly rotationally excited molecules to the superspecular direction indicates that momentum perpendicular to the surface is more efficiently converted to rotation (and coupled to the surface) than the parallel component of the momentum. This effect was first observed by Kleyn, Luntz, and Auerbach[36] in the scattering of NO from Ag(111). Interestingly, even molecules that convert almost all of their incident translational energy into rotation display this preferential momentum conversion.

### C. Surface temperature dependence

As can be seen from Figs. 10 and 11, the rotational distribution of desorbing CO molecules is well described by a Boltzmann distribution characterized by a temperature that is $0.82 \pm 0.08$ of the surface temperature. This observation does not indicate that desorbing molecules have not fully equilibrated with the surface; instead, it indicates that rotational-to-translational energy conversion is important in the desorption process as well as the sticking process. Much in the same way that rotationally trapped molecules are able to kick themselves off the surface in a multiple-bounce trajectory, chemisorbed molecules can use their rotational energy to leave the surface. In doing so, their rotational energy, which was initially determined by the surface temperature, is cooled in the desorption process. This effect, often termed *rotational cooling*, was also observed by Muhlhausen *et al.*[23] in their simulations of NO desorbing from Ag(111).

This effect can also be understood using detailed balance arguments.[37] If the sticking coefficient for CO on Ni(111) were unity, the rotational distribution of the desorbing flux would perforce be a Boltzmann distribution at the surface temperature. The CO/Ni(111) sticking coefficient is, however, less than one at all incident energies.[3] Because the scattered molecules are highly rotationally excited, it follows by detailed balance that the desorbing molecules must be rotationally cool.

The effect of surface temperature on the scattered molecules is less clear. The analysis presented in Sec. III D 2 suggests that the scattering distribution is relatively insensitive to surface temperature and the observed temperature dependence is due to contributions from the desorption channel. A satisfactory fit to the observed data could be produced only with a desorption temperature that was somewhat higher than the observed temperature. This discrepancy is small and is just within the error bars of the measurements, but we cannot rule out a weak correlation between the scattered rotational distribution and the surface temperature. To resolve this question more fully, a measurement of the relative intensities of the flux at different angles is necessary.

## V. SUMMARY AND CONCLUSIONS

We have measured the angularly resolved rotational state distributions of CO scattered and desorbed from a single crystal Ni(111) surface using (2+1) resonance-enhanced multiphoton ionization. CO molecules that scattered from the Ni(111) surface had highly non-Boltzmann rotational state distributions that were dependent on the incident translational energy and the final scattering angle.

Effects of the orientational anisotropy of the CO/Ni(111) potential were seen in the rotational state distributions of the scattered CO molecules. First, up to total translational-to-rotational energy conversion was observed in the scattering process. This effect was interpreted by considering *rotational trapping* that resulted from the strongly attractive interaction between the C end of the CO molecule and the Ni(111) surface. Because the highest observed rotational state was determined by the *total* incident momentum rather than the component of the incident momentum normal to the surface, the corrugation of the Ni(111) surface must be important in the scattering process. Second, in the far superspecular direction, the rotational state distributions were bimodal. The high-$J$ maximum was attributed to a *rotational rainbow* from the weakly attractive interaction of the O end of the CO molecule with the Ni(111) surface. The position of the rotational rainbow was seen to scale with incident translational energy. Additionally, the highest degree of rotational excitation was found in molecules scattered to the far superspecular direction. This behavior indicated that momentum perpendicular to the surface is more efficiently coupled to rotation (and the surface) than momentum parallel to the surface. Surface temperature had little effect on the scattered rotational state distribution.

These measurements indicate that the scattering dynamics of CO from a Ni(111) surface differ substantially for the two ends of the molecule. Molecules that are incident O end down preferentially scatter from the surface, as this orientation is only weakly attractive. On the other hand, those molecules that are incident in the strongly attractive C-end-down configuration are much more likely to stick to the surface and later desorb.

CO molecules that are first trapped on the surface and later desorb were preferentially detected along the surface normal. The rotational state distributions of desorbing molecules were well fit by Boltzmann distributions with a characteristic temperature that was $0.82 \pm 0.08$ of the surface temperature.

## ACKNOWLEDGMENTS

MAH thanks Sylvia T. Ceyer for many insightful discussions on this topic. This work was supported by the Office of Naval Research under Grant No. N0014-91-J-1023 and by the National Science Foundation under Grant No. DMR-90-14367.

[1] For an excellent review of progress in this field, see J. A. Barker and D. J. Auerbach, Surf. Sci. Rep. **4**, 1 (1985).
[2] A. W. Kleyn and T. C. M. Horn, Phys. Rep. **4**, 191 (1991).

[3] S. L. Tang, J. D. Beckerle, M. B. Lee, and S. T. Ceyer, J. Chem. Phys. **84**, 6488 (1986).
[4] H. P. Steinrück, A. Winkler, and K. D. Rendulic, Surf. Sci. **152/153**, 323 (1985).
[5] J. B. Miller, H. R. Siddiqui, S. M. Gates, J. N. Russel, Jr., J. T. Yates, Jr., J. C. Tully, and M. J. Cardillo, J. Chem. Phys. **87**, 6725 (1987).
[6] S-S. Sung and R. Hoffmann, J. Am. Chem. Soc. **107**, 578 (1985).
[7] J. Yoshinobu, R. Zenobi, J. Xu, Z. Xu, and J. T. Yates, Jr., J. Chem. Phys. **95**, 9393 (1991).
[8] G. D. Kubiak, J. E. Hurst, H. G. Rennagel, G. M. McClelland, and R. N. Zare, J. Chem. Phys. **79**, 5163 (1983).
[9] G. O. Sitz, A. C. Kummel, and R. N. Zare, J. Chem. Phys. **89**, 2558 (1988).
[10] M. A. Hines, Ph.D. thesis, Stanford University, 1991.
[11] W. Braker and A. L. Mossman, *Matheson Gas Data Book*, 6th ed. (Matheson, Secaucus, NJ, 1980), p. 130.
[12] M. A. Hines, H. A. Michelsen, and R. N. Zare, J. Chem. Phys. **93**, 8557 (1990).
[13] T. A. Spiglanin, R. A. Perry, and D. W. Chandler, J. Chem. Phys. **87**, 1568 (1987).
[14] R. G. Bray and R. M. Hochstrasser, Mol. Phys. **31**, 1199 (1976).
[15] P. Marchand and L. Marmet, Rev. Sci. Instrum. **54**, 1034 (1983).
[16] A. W. Kleyn, A. C. Luntz, and D. J. Auerbach, Phys. Rev. Lett. **47**, 1169 (1981).
[17] R. J. Behm and C. R. Brundle, J. Vac. Sci. Technol. A **2**, 1040 (1984).
[18] See, e.g., M. Asscher, W. L. Guthrie, T. -H. Lin, and G. A. Somorjai, J. Chem. Phys. **78**, 6992 (1983); J. Segner, H. Robota, W. Vielhaber, G. Ertl, F. Frenkel, J. Häger, W. Krieger, and H. Walther, Surf. Sci. **131**, 273 (1983); D. C. Jacobs, K. W. Kolasinski, S. F. Shane, and R. N. Zare, J. Chem. Phys. **91**, 3182 (1989); R. J. Hamers, P. L. Houston, and R. P. Merrill, *ibid.* **88**, 6548 (1988); D. A. Mantell, S. B. Ryali, G. L. Halter, and J. B. Fenn, *ibid.* **78**, 4520 (1983).
[19] R. D. Levine and R. B. Bernstein, *Molecular Reaction Dynamics* (Clarendon, New York, 1974), p. 59.
[20] Of course, the aesthetic part of the optical rainbow, the separation of colors, results from the fact that the index of refraction of water is wavelength dependent, which is unrelated to the scattering singularity.
[21] C. T. Rettner, J. Kimman, and D. J. Auerbach, J. Chem. Phys. **94**, 735 (1991).
[22] K. R. Lykke and B. D. Kay, J. Phys. Condensed Matter **3**, S65 (1991).
[23] C. W. Muhlhausen, L. R. Williams, and J. C. Tully, J. Chem. Phys. **83**, 2594 (1985).
[24] G. O. Sitz, A. C. Kummel, and R. N. Zare, J. Chem. Phys. **89**, 2558 (1988).
[25] A. C. Kummel, G. O. Sitz, R. N. Zare, and J. C. Tully, J. Chem. Phys. **89**, 6947 (1988); **91**, 5793 (1989).
[26] J. C. Polanyi and R. J. Wolf, Ber. Bunsenges. Phys. Chem. **86**, 356 (1982); J. C. Polanyi and R. J. Wolf, J. Chem. Phys. **82**, 1555 (1985).
[27] D. C. Jacobs and R. N. Zare, J. Chem. Phys. **91**, 3196 (1989).
[28] J. Harris and A. C. Luntz, J. Chem. Phys. **91**, 6421 (1989).
[29] E. W. Kuipers, M. G. Tenner, A. W. Kleyn, and S. Stolte, Phys. Rev. Lett. **62**, 2152 (1989).
[30] G. H. Fecher, N. Böwering, M. Volkmer, B. Pawlitzky, and U. Heinzmann, Surf. Sci. **230**, L169 (1990).
[31] D. J. Doren and J. C. Tully, J. Chem. Phys. **94**, 8428 (1991).
[32] S. L. Tang, M. B. Lee, Q. Y. Yang, J. D. Beckerle, and S. T. Ceyer, J. Chem. Phys. **84**, 1876 (1986).
[33] X. D. Zhu, Th. Rasing, and Y. R. Shen, Phys. Rev. Lett. **61**, 2883 (1988).
[34] J. A. Barker, A. W. Kleyn, and D. J. Auerbach, Chem. Phys. Lett. **97**, 9 (1983).
[35] T. Brunner and W. Brenig, Surf. Sci. **261**, 284 (1992).
[36] A. W. Kleyn, A. C. Luntz, and D. J. Auerbach, Surf. Sci. **117**, 33 (1982).
[37] An excellent introduction to the intricacies of detailed balance can be found in M. J. Cardillo, M. Balooch, and R. E. Stickney, Surf. Sci. **50**, 263 (1975).